Available online at www.sciencedirect.com
SCIENCE DIRECT®
Journal of Nuclear Materials 340 (2005) 149–162
journal of nuclear materials
www.elsevier.com/locate/jnucmat

Elemental dissolution study of Pu-bearing borosilicate glasses

D.M. Wellman *, J.P. Icenhower, W.J. Weber

Pacific Northwest National Laboratory, P.O. Box 999, Richland, WA 99352, USA

Received 10 May 2004; accepted 29 October 2004

Abstract

Single-pass flow-through tests were conducted to study the effects of self-radiation damage from alpha decay on dissolution kinetics of three radiation-aged Pu-bearing (1 mass% PuO_2) borosilicate glasses over a pH interval of 9–12 at 80–88 °C. The chemical compositions of the glasses were identical except the $^{239}Pu/^{238}Pu$ isotopic ratio, which was varied to yield accumulated doses of 1.3×10^{16}, 2.9×10^{17} and 2.6×10^{18} α-decays/g at the time of testing. Release of Al, B, Cs, Na, Si and U to solution increased with increasing pH, whereas Ca, Pu and Sr were invariant over the pH interval. Average dissolution rates, based on B release, were identical within experimental uncertainty for all three glass compositions and increased from 0.17 ± 0.07 at pH(23 °C) 9 to 10.6 ± 2.7 (g/(m^2 d^1)) at pH(23 °C) 12. Release rates of Pu were 10^2- to 10^5-fold slower compared to all other elements and were not affected by isotopic composition, self-radiation damage sustained by the glass, or pH. These data demonstrate that self-radiation damage does not affect glass dissolution rates, despite exposure to internal radiation doses for >20 years.
Published by Elsevier B.V.

1. Introduction

Although the corrosion resistance of borosilicate glass has been studied extensively [1–10], relatively few investigations have been able to quantitatively assess the effect of self-radiation damage on the dissolution rate. Within this limited set of studies there is a dispersion of opinion regarding the extent to which radiation damage affects element release rates. An increase in dissolution rate due solely to radiation self-damage must be de-convoluted from the contributions of radiolytic effects and experimental artifacts; typically, this is difficult. For example, Wronkiewicz et al. [11] reported that rates of secondary phase formation on a transuranic-bearing glass increased by a factor of 4 due to radiation effects. This conclusion accords with that of Weber et al. [12], in which static tests were conducted on newly prepared ^{238}Pu-, ^{239}Pu- and ^{232}Th-bearing glass coupons. A 2- to 3-fold increase in dissolution was reported for the ^{238}Pu-bearing compared to ^{239}Pu- and ^{232}Th-bearing specimens. However, because the glasses had not accumulated appreciable self-radiation damage, the increase was attributed to the buildup of radiolysis products in the surrounding solution of the ^{238}Pu-bearing compared to the ^{239}Pu- and ^{232}Th-bearing tests, rather than to direct, self-inflicted radiation damage. Further, Wronkiewicz [11] concluded from a survey of literature that a reported 10- to 15-fold increase in rates occurred in static experiments in which surface area to volume (S/V) ratios were low. Part of this rate increase was, therefore, attributed to radiation damage, but the rest to the influence of radiolytic products in thin water films coating the glass specimens. In contrast, Advocat et al. [2] and Werme et al. [13] reported statistically insignificant

* Corresponding author. Tel.: +1 509 375 2017.
E-mail address: dawn.wellman@pnl.gov (D.M. Wellman).

0022-3115/$ - see front matter Published by Elsevier B.V.
doi:10.1016/j.jnucmat.2004.10.166

change in dissolution rates between actinide-doped and non-radioactive analog glasses.

Part of the ambiguity in these investigations may arise from the comparison of actinide-doped and non-radioactive glasses, which differ in composition and in factors related to processing. However, there is a significant contribution to the uncertainty from the manner in which dissolution studies have been conducted. For example, in nearly all of the tests surveyed, rates were determined from static reactor systems. This setup has a number of disadvantages relative to flow tests, at least for obtaining the critical data sought here. First, because the solution in contact with glass is never refreshed, the saturation state of the solution in the static tests changes with time. As dissolved components of the glass accumulate in solution, the chemical affinity (which is a measure of departure from equilibrium) changes with reaction progress. Thus, dissolved elements, such as Al and Si, play a progressively larger role in diminishing the dissolution rate. Depending on factors related to the chemistry of the glass, the rate may decrease by up to a factor of 10^4 [6]. On the other hand, solution pH may increase as alkali cations in glass (e.g., Li^+, Na^+, K^+) exchange with H_3O^+ from water. Alkali-rich glasses have been selected as a disposal medium in a number of United States Department of Energy sites and these waste forms appear to be most vulnerable to exchange reactions [14]. Second, in static tests in which the ratio of glass surface area to solution volume (SA/V) is large, radioactive decay will produce a number of radiolysis products in the solution. For alpha-particle emitting actinides, formation of H_2, H_2O_2, $HO_2^{\cdot}$ and $^{\cdot}OH$ from interaction with water may cause acceleration of the glass reaction rate either by imposing a higher oxidation state or by shifting the solution pH [11]. In the first case, elements that are reduction–oxidation (redox) sensitive, such as U and Pu, may be released to solution faster than anticipated. In the second instance, solution pH can increase over time as radioactive decay of elements in solution directly breaks down buffering agents or from the buildup of radiolysis products, such as $^{\cdot}OH$, in the solution. Therefore, ample reason exists to suspect that the presence of radiolysis products in static or slowly-replenished flow-through experiments can yield accelerated rates of reaction making it difficult to disentangle from these data the relative contribution of self-radiation damage to glass.

Data are presented from single-pass flow-through (SPFT) tests on the dissolution kinetics of a radiation-aged chemically complex borosilicate glass series that contain a total of 1.0 mass% PuO_2. Within the series, proportions of ^{238}Pu to ^{239}Pu were varied: DRG-1 glass contains 1.0 mass% $^{239}PuO_2$, DRG-2 glass contains 0.9 mass% $^{238}PuO_2$ and 0.1 mass% $^{239}PuO_2$ and DRG-3 glass contains 1.0 mass% $^{238}PuO_2$. Varying the isotopic composition of the glass series yielded an accumulated dose ranging from 1.3×10^{16} to 2.6×10^{18} α-decays/g over a time interval of ~21 years. The response of the corrosion resistance of the glass specimens to radiation damage was tested over a pH(23 °C) interval of 9–12 and at temperatures between 80 °C and 88 °C. Because the solution in the reaction vessel was continuously replenished, radiolysis products and dissolved glass components were not allowed to build up and the solution pH was maintained at constant values. Thus, radiolysis effects, as observed in earlier static tests [12], were minimized. Under these conditions, the release of elements from each glass was statistically identical at each pH value, despite the difference in accumulated radiation damage from alpha decay of the plutonium isotopes. Thus, the results of the tests present strong evidence that the dissolution rate is unaffected by the amount of self-radiation damage imparted to it by prolonged exposure to alpha radiation.

2. Methods

2.1. Preparation and characteristics test material

A simulated borosilicate waste glass (MCC defense reference glass), with the composition given in Table 1 [12] was used as the starting glass. The glass was prepared by first mixing reagent grade oxides, hydroxides, and carbonates to the desired concentrations and then using multiple melt processing steps to form a large homogeneous quantity (several kilograms) of glass. The composition was confirmed via inductively coupled plasma-optical emission spectroscopy and inductively coupled plasma-mass spectrometry of a sub-sample of the glass subjected to acid digestion. In July, 1982, three

Table 1
Nominal chemical composition of simulated waste glass in mass% oxide

Oxide	Nominal concentration (mass%)
SiO_2	49.6
B_2O_3	7.0
Al_2O_3	6.0
CaO	2.0
Fe_2O_3	10.0
Li_2O	4.9
MgO	0.7
MnO_2	3.0
Na_2O	9.1
NiO	2.0
SrO	0.5
ZrO_2	0.7
Cs_2O	0.5
U_3O_8	3.0
$^{239}Pu/^{238}Pu$: PuO_2	1.0

Weber et al. [12]

sample batches of this glass were doped with approximately 1.0 wt% PuO_2 accordingly to the MCC-6 method for preparation of actinidedoped waste forms [12]. Because of the same starting glass composition, this processing procedure ensured identical sample compositions in which the α-activity of each glass sample was altered by varying the $^{239}Pu/^{238}Pu$ isotopic ratio in the PuO_2 dopant used. The PuO_2 was added as a nitric acid solution to the base composition of the simulated waste glass. The mixture was dried on a hot plate, melted at 1200 °C, poured into bars and annealed at 500 °C. Interested readers should consult Weber et al. [12], and references therein, for additional details regarding the preparation and characterization of the glass specimens.

As a result of the difference in the isotopic ratio of $^{239}Pu/^{238}Pu$, the accumulated dose, imparted by alpha decay over time, varied by a factor of about 200 as listed in Table 2. The calculation of accumulated dose is based on radiochemical analysis of the ^{238}Pu and ^{239}Pu content in the originally prepared samples [12]. Photomicrographs, representative of each glass composition, were taken of the glass coupons after being cut and polished prior to testing (Fig. 1). The images clearly indicate that as the accumulated dose (^{238}Pu content) increases there is increased etching and loss of transparency of the glass coupons, which is commonly cited as evidence for radiation damage.

2.2. Dissolution tests

Dissolution rates were determined as a function of pH over the pH(23 °C) interval of 9–12. Dissolving *tris(hydroxymethyl)aminomethane* (TRIS) buffer in deionized water (DIW) formed the base mixture for 0.05 M pH(23 °C) 9 and 10 solutions. Concentrated spectroscopic grade nitric acid (HNO_3) and high purity lithium hydroxide (LiOH) were used to adjust the solutions to the target pH values of 9 and 10, respectively. Alkaline solutions at pH(23 °C) 11 and 12 were prepared by mixing LiOH with DIW; LiCl was used as a background solute. The four solution compositions and their in situ pH values at 80 °C and 88 °C were calculated using the thermodynamic software package EQ3/6 [15] and are listed in Table 3. It is important to note the change in the in situ pH of the experiment because, as is evident in Table 3, the pH can vary by as much as 1.3 pH units over the temperature interval of 23–88 °C.

The dissolution kinetics of the Pu-bearing glass samples was determined using single-pass flow-through (SPFT) apparatus at a target temperature of 90 °C and flow rate of 60 mL d^{-1}. Target flow rates used in this investigation (60 mL d^{-1}) were selected to ensure that the system would be far from saturation and near the forward rate of reaction (i.e. the maximum dissolution rate) [16,17]. A 60 mL d^{-1} flow rate ensured exchange of one reactor volume per day and prevented buildup of dissolved glass components and potential radiolysis products in solution. The SPFT apparatus, illustrated schematically in Fig. 2, consists of a computer programmable syringe pump (Kloehn; model 50300) that transfers solution from an influent reservoir to Teflon® reactors. The reactors are *perfluoroalkoxy* (PFA) (Savillex) vessels that consist of a top and bottom piece that, when screwed together, forms a ~40 mL capacity jar. The top half contains ports for the ingress of input and the egress of effluent solutions. A titanium assembly that suspends the glass coupon specimens (see below) to mid-reactor height fits into the bottom half. The reactors sit in custom-machined recessed cavities in an aluminum heater block assembly that in turn resides in a dry bath incubator (Boekel Scientific). The temperature of the dry bath was set to 90 °C and controlled using a microprocessor-based temperature controller (Watlow; model 987). Because the dry bath assembly was situated inside a fume hood, in which the volume of air was rapidly exchanged, the heater blocks could not maintain the target temperature. The temperature of the solution within the reactors was measured with a digital thermocouple (Glas-Col; model TC105) accurate to within ±2 °C; actual temperatures measured within the reactors during each test (80–88 °C) are listed in Table 4. The syringe pumps were configured so that four experiments, one for each glass composition plus a control, could be run simultaneously using the same influent solution. Transport of influent from the feed reservoir and effluent solution to collection vials was accommodated by 1.59 mm Teflon tubing for pH(23 °C) 9–11 experiments. The low solubility of plutonium-hydroxides in alkaline solutions coupled with the significantly lower temperature encountered within the effluent transfer tubing, relative to that within the reactors, led to concern regarding

Table 2
Isotopic composition, accumulated dose and density measurements for Pu-bearing glasses

Sample	Target dopant (mass%)	Measured concentration (mass%)	Accumulated dose (α-decays/g)	Original density (g/cm^3)[a]
DRG-P1	1.0 $^{239}PuO_2$	0.95 $^{239}PuO_2$	1.3×10^{16}	2.77
DRG-P2	0.9 $^{239}PuO_2$, 0.1 $^{238}PuO_2$	0.95 $^{239}PuO_2$ 0.08 $^{238}PuO_2$	2.9×10^{17}	2.77
DRG-P3	1.0 $^{238}PuO_2$	0.08 $^{238}PuO_2$ 0.77 $^{238}PuO_2$	2.6×10^{18}	2.77

[a] Weber et al. [12]

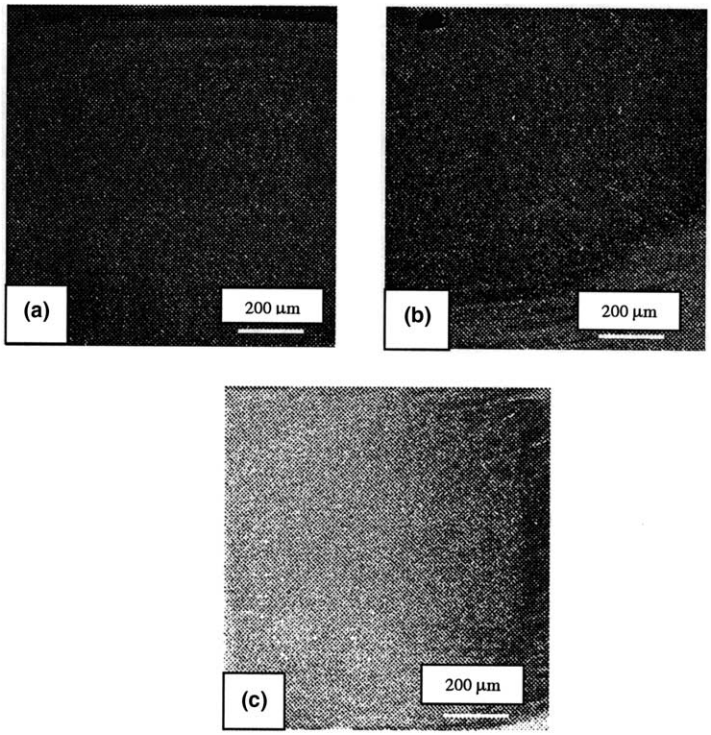

Fig. 1. Photomicrographs of DRG-P test glass samples: (a) DRG-P1, (b) DRG-P2 and (c) DRG-P3. Note the visible increase in etching of the coupons with increasing ^{238}Pu isotopic content.

Table 3
Composition of solutions used in SPFT experiments. Solution pH values 25 °C< were calculated with EQ3NR Code V7.2b database [15]

Solution #	Composition	pH (23 °C)	pH (80 °C)	pH (88 °C)
1	0.05 M TRIS + 0.004 M HNO_3	9.1	7.9	7.8
2	0.05 M TRIS + 0.003 M LiOH	10.0	8.7	8.6
3	0.0107 M LiOH + 0.010 M LiCl	11.0	10.2	10.1
4	0.0207 M LiOH + 0.010 M LiCl	12.0	10.9	10.7

precipitation within the tubing. Precipitation within the 1.59 mm Teflon tubing could block the flow of effluent solution causing back-flow of solution, increased pressure within the flow system, erroneous flow rates (and subsequent dissolution rates), or premature termination of the test. To circumvent this possibility, 3.17 mm Teflon tubing was used to transfer solution in experiments conducted at pH(23 °C) 12.

The Teflon reactors were lined with platinum inserts to minimize potential experimental artifacts, such as fluoride formation from radiation damage imparted to the reactors. The presence of fluoride species could disproportionately reduce the solution pH in tests with the three glass compositions and thereby skew the results. However, Teflon influent and effluent solution transfer lines were in contact with the solution within the reactor and could serve as a source of fluoride, which could affect rates. This possibility is considered below.

Each reactor tested four compositionally identical Pu-bearing glass coupons (~9 mm × 10 mm × 1.5 mm each) that rested on a grated titanium basket submerged within the Pt-lined reactor (Fig. 2 inset). This configuration allows the influent solution to contact the maximum coupon surface area. The coupons, which had not been previously exposed to aqueous solutions, were gently cleaned with an alcohol-wetted paper laboratory wipe to remove any loose material from the surface. Effluent solution continuously flowed out of the reactors and was collected in vials next to the heating unit. Experiments were run until steady-state conditions (constant element concentrations over time) prevailed, which was approx-

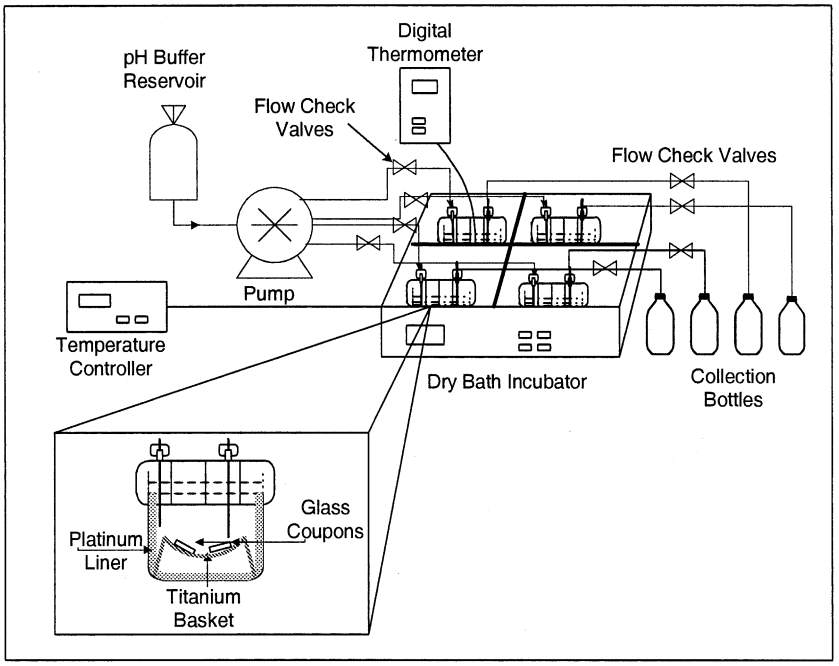

Fig. 2. Schematic of the single-pass flow-through (SPFT) apparatus and enlarged view of Teflon reactor configuration including the non-reactive glass coupon holder. (Note the schematic is not drawn to scale).

imately 10 days or the time necessary to exchange ~10 reactor volumes.

Three blank samples were drawn prior to addition of the glass coupons and a control experiment was run at all test pH values. The control tests were configured the same as the experiments, but were devoid of test glass coupons. The control tests provided the correction values for background element concentrations in the effluent solution and demonstrated that there were no systematic sources of contamination. Aliquots of effluent solution were periodically checked to ensure pH stability; measured effluent pH was within ±0.05 pH units of the influent value, which is well within the informal in-house established uncertainty of ±0.2 pH units. The constant pH values indicate that unwanted fluoride species were not present (at least in significant amounts) within the flow-through system Concentrations of Si, Ca, Na, Al, B, Sr and Cs were determined by inductively coupled plasma-optical emission spectroscopy (ICP-OES). Effluent concentrations of Pu and U were determined by inductively coupled plasma-mass spectrometry (ICP-MS).

The scope of this investigation is concerned only with the *total* release of plutonium, irrespective of form (dissolved or colloidal). It is well known that a fraction of released plutonium may occur as colloidal material [18–20], particularly at the high pH values. Therefore, the effluent samples from the pH(23 °C) 12 tests were filtered through 0.45 μm Nalgene® filters to segregate colloidal from dissolved Pu. The effluent chemistries of the filtered and unfiltered aliquots were compared to each other and Pu concentrations are equivalent within error (see 'Results'), indicating that Pu is most likely in a dissolved form in all samples.

3. Dissolution rates and error calculations

Dissolution rates obtained from the SPFT tests are based on steady-state element concentrations in the effluent solution. The rates are normalized to the element mass fraction present in the glass composition by the following formula:

$$r_{i,j} = \frac{(C_{i,j} - \overline{C}_{i,b})q_j}{f_i S_j}, \tag{1}$$

where $r_{i,j}$, is the normalized release rate (g/m^2 d) based on element i at the jth sampling, C_i is the concentration (g L^{-1}) of the element of interest, i, in the effluent at the jth sampling, $\overline{C}_{i,b}$ is the average background concentration (g L^{-1}) of the element i in the influent, q is the flow rate (L d^{-1}) at the jth sampling, f_i is the mass fraction of the element in the sample (dimensionless) and S_j is the total surface area (m^2) of the test coupons. In cases where the analyte concentration was below the detection threshold, the background concentration of the element (from the control experiments or from aliquots of the starting solution, whichever was higher) was set at the value of the detection threshold providing a maximum

Table 4
Experimental conditions and steady-state element concentrations for DRG-P glasses

Sample: DRG-	Temp (°C)	Average effluent (pH)	Avg. flow rate (mL/d)	Surface area $\times 10^4$ (m^2)[a]	Average [Al] $\times 10^4$ (g/L)	Average [B] $\times 10^4$ (g/L)	Average [Na] $\times 10^4$ (g/L)	Average [Si] $\times 10^4$ (g/L)	Average [Sr] $\times 10^5$ (g/L)	Average [Ca] $\times 10^5$ (g/L)	Average [Cs] $\times 10^5$ (g/L)	Average [U] $\times 10^5$ (g/L)	Average [Pu] $\times 10^7$ (g/L)
P1-E1	80	9.1	56	9.45	1.85	1.15	39.7	1.31	2.54	9.72	2.60	7.72	5.76
P2-E1	81	9.1	56	9.66	2.29	1.13	41.5	1.27	2.65	10.0	2.53	12.6	2.09
P3-E1	80	9.1	56	9.38	1.88	1.07	38.3	1.25	2.51	9.59	2.46	7.35	5.97
P1-E2	88	10.0	50	9.31	5.65	3.44	139	3.74	6.04	22.0	6.91	46.2	9.36
P2-E2	88	10.0	28	9.53	3.97	3.97	150	4.39	7.23	27.6	7.89	40.8	3.56
P3-E2	88	10.0	44	9.83	6.30	3.94	156	4.32	6.80	24.0	7.77	48.7	3.83
P1-E3	82	11.0	74	8.56	11.9	8.03	268	8.42	5.04	23.5	17.7	23.0	3.45
P2-E3	82	11.0	79	9.02	8.74	6.44	195	6.30	4.46	22.3	12.1	19.4	6.20
P3-E3	82	11.0	55	9.09	12.7	8.43	299	9.14	5.75	27.1	19.6	21.4	<0.50[b]
P1-E4	85	12.0	59	9.16	44.1	3.15	983	29.7	3.74	18.2	59.9	231	1.21
P2-E4	85	12.0	67	9.39	29.5	6.90	505	16.0	3.62	19.1	33.2	139	3.62
P3-E4	84	12.0	60	8.30	60.7	38.4	1130	34.4	3.46	16.1	66.4	255	<0.50[b]

[a] Surface area was the total surface area calculated for four pristine coupons.
[b] Analyte was below detection threshold value.

threshold value. The detection threshold of any element is defined as the lowest concentration calibration standard that can be determined reproducibly during an analytical run within 10%. Flow rates were determined by gravimetric analysis of the fluid collected at each sampling interval. The value of f_i is calculated from the chemical composition of the glass [12].

The surface area of the coupons used in the dissolution experiments was calculated based on coupon dimensions measured using a custom-built laser surface profilometer system. The system provides precise three-dimensional measurements of the coupon dimensions by utilizing a series of lasers, point sensors and diode array detectors to scan along the *x*-, *y*- and *z*-axes. The apparatus was originally designed to accurately determine surface areas of highly radioactive ceramic specimens with a minimum exposure to investigators, which, of course, had a similar usefulness in this investigation. Interested readers should consult Strachan et al. [21] for a detailed description of the profilometer system. The measured surface areas of the coupons are listed in Table 4. The total surface area of the multiple coupons in each experiment (typically 4) was obtained by summing the surface areas of the glass specimens.

In addition to the measured coupon dimensions, the mass of the coupons was determined using a three-place analytical balance. These data were used to calculate the densities of the glass coupons, which were compared to independent density measurements obtained through helium pycnometry. The difference between the calculated and measured densities of the coupons was within 5%; thus, it was assumed the surface area of the coupons was accurately calculated.

Determining the standard deviation of the dissolution rates requires accounting for the uncertainty associated with each parameter in Eq. (1). The standard deviation of a function for uncorrelated random errors is given by:

$$\sigma_f = \sqrt{\sum_{i=1}^{n} \left(\frac{\partial f}{\partial x_i}\right)^2 \sigma_i^2}, \tag{2}$$

where σ_f is the standard deviation of the function f, x_i is the parameter i and σ_i is the standard deviation of parameter i.

Substituting Eq. (1) in (2) and converting to relative standard deviations, $\widehat{\sigma}_r$, yields:

$$\widehat{\sigma}_r = \sqrt{\frac{(\widehat{\sigma}_c c_i^{\text{out}})^2 + (\widehat{\sigma}_b c_i^{\text{in}})}{(c_i^{\text{out}} + c_i^{\text{in}})^2} + \widehat{\sigma}_{fi}^2 + \sigma_S^2 + \sigma_q^2}. \tag{3}$$

Errors for $\widehat{\sigma}_c$, $\widehat{\sigma}_b$, $\widehat{\sigma}_{fi}$, $\widehat{\sigma}_S$ and $\widehat{\sigma}_q$ are 10%, 10%, 3%, 5% and 5%, respectively. This approach to error analysis results in typical 2σ uncertainties of approximately ±20% to 40% for SPFT-measured dissolution rates.

4. Scanning electron microscopy

Surface features of pre- and post-reacted test coupons were investigated using scanning electron microscopy (SEM). Photomicrographs were obtained by a JEOL 840 SEM equipped with a Robinson 6.0 backscatter detector and GATAN DM software version 3.2, 1996. The beam conditions were 20 KeV potential and a 1 nanoamp beam current. While attempts were made to document the reaction products on the glass specimen surfaces, the intense radiation field produced by the presence of Pu precluded complete energy dispersive spectrometry (EDS) characterization.

5. Results

Experimental conditions, including temperature, solution pH, flow rates, total specimen surface area and steady-state effluent chemistries are listed in Table 4. Target flow rates used in this investigation (60 mL d^{-1}) were selected to ensure that the system would be far from saturation and near the forward rate of reaction (i.e. the maximum dissolution rate). Experiments were monitored until steady-state conditions were achieved; i.e., ensuring effluent pH and element concentrations were invariant with respect to time. Fig. 3 illustrates, based on effluent boron concentrations from a test with DRG-P1, that steady-state conditions were achieved at all four pH conditions. The pattern of results depicted in this figure is representative of element release rates from each glass composition.

5.1. Effects of PH

Experiments were conducted over a set of pH(T) values between 7.8 and 10.7 (pH(23 °C) 9–12). Dissolution rates, with accompanying uncertainty estimates, were calculated from steady-state concentrations of elements in effluent solutions and are listed in Table 5. Fig. 4(a)–(c) illustrate the rate dependence on solution pH(T). As previously discussed, the in situ pH(T) of the solutions at temperature was calculated using the EQ3NR program (Table 3). In general, Fig. 4(a)–(c) indicate that for each glass composition the dissolution rates based on Al, B, Cs, Na, Si and U are identical within experimental uncertainty. Because boron release is not modified by formation of secondary phase products, the rate with respect to boron best quantifies the dissolution. Fig. 5 is a plot of the dissolution rate based solely on boron and indicates that all glass compositions dissolve at the same rate over the pH interval, irrespective of accumulated radiation damage. Rate data show that as the pH(T) increases from 7.8 to 10.7, the average rate increases from 0.17 ± 0.07 to 10.6 ± 2.7 (g/(m^2 d^1)). Linear regression of the data for each composition yields an average slope that quantifies the dependence of the rate on pH, which is designated as η, the power law coefficient. The values of $\eta = 0.54(\pm 0.04)$, $0.58(\pm 0.04)$ and $0.58\ (\pm 0.04)$ (dimensionless), were obtained for DRG-P1, DRG-P2 and DRG-P3, respectively. These values are similar, although slightly higher, than those reported for other borosilicate glass compositions [22–24] and silicate minerals [25].

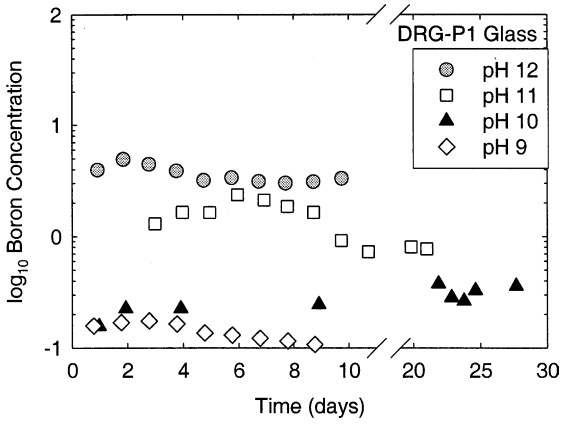

Fig. 3. Plot of $\log_{10}$ boron concentration versus time for SPFT experiments with DRG-P1 glass as a function of pH. Boron release data indicate that all experiments reach steady-state conditions by 10 days. Note the scale break.

In contrast to the behavior of Al, B, Cs, Na and Si, release of Ca and Sr show no dependence on solution pH (Fig. 4(a)–(c)). Although rates based on all elements are identical within error at pH(23 °C) = 9 (except Pu; see below), rates based on Ca and Sr are relatively slow compared to other rates as the solution pH increases. The relative difference in rates is a reflection of the lack of pH dependence for Ca and Sr release. The magnitude of the rate difference between Ca and Sr on the one hand and Al, B, Cs, Na and Si on the other, at pH(23 °C) = 12 is greater than the accumulated uncertainty of the values. Thus, behavior of Ca and Sr appears to be different from the rest of the elements.

Uranium rates generally increase with solution pH; rates at pH(23 °C) 9, 10 and 12 are the same within experimental error to those of Al, B, Cs, Na and Si. However, U rates at pH(23 °C) = 11 are anomalously slow for all three glass compositions. The unexplained behavior of U at pH(23 °C) = 11 forces slopes of the regression lines for each glass composition to lower values. The relatively low values of η obtained from U release are thus an artifact of this anomalous behavior.

Evidence for relatively slow release of Pu compared to the other elements ($10–10^3$ times) is not likely a reflection of experimental artifacts (Fig. 4(a)–(c)). As in the cases of Ca and Sr, Pu rates are constant or decrease slightly across the pH range studied. Thus, the difference in rates between B and Pu increases with

Table 5
Calculated dissolution rates for DRG-P glasses in g/(m^2 d). Numbers in parentheses are 2σ uncertainties (also in g/(m^2 d)) on the rate values

Sample: DRG-	PH	Al rate	B rate	Na rate	Si rate	Sr rate	Ca rate	Cs rate	U rate	Pu rate
P1-E1	9.1	3.34×10^{-01} ($\pm8.56\times10^{-02}$)	1.76×10^{-01} ($\pm7.30\times10^{-02}$)	3.25×10^{-01} ($\pm8.55\times10^{-02}$)	2.06×10^{-01} ($\pm5.21\times10^{-02}$)	4.34×10^{-01} ($\pm1.10\times10^{-01}$)	1.94×10^{-01} ($\pm9.48\times10^{-02}$)	3.23×10^{-01} ($\pm8.17\times10^{-02}$)	1.78×10^{-01} ($\pm4.51\times10^{-02}$)	3.50×10^{-03} ($\pm9.39\times10^{-04}$)
P2-E1	9.1	4.07×10^{-01} ($\pm1.04\times10^{-01}$)	1.67×10^{-01} ($\pm7.05\times10^{-02}$)	3.34×10^{-01} ($\pm8.78\times10^{-02}$)	1.91×10^{-01} ($\pm4.85\times10^{-02}$)	4.55×10^{-01} ($\pm1.15\times10^{-01}$)	2.02×10^{-01} ($\pm9.58\times10^{-02}$)	3.09×10^{-01} ($\pm7.81\times10^{-02}$)	2.89×10^{-01} ($\pm7.29\times10^{-02}$)	1.05×10^{-03} ($\pm2.97\times10^{-04}$)
P3-E1	9.1	3.42×10^{-01} ($\pm8.76\times10^{-02}$)	1.54×10^{-01} ($\pm6.68\times10^{-02}$)	3.14×10^{-01} ($\pm8.28\times10^{-02}$)	1.91×10^{-01} ($\pm4.84\times10^{-02}$)	4.29×10^{-01} ($\pm1.09\times10^{-01}$)	1.90×10^{-01} ($\pm8.91\times10^{-02}$)	3.08×10^{-01} ($\pm7.79\times10^{-02}$)	1.73×10^{-01} ($\pm4.36\times10^{-02}$)	3.71×10^{-03} ($\pm1.01\times10^{-03}$)
P1-E2	10.0	8.61×10^{-01} ($\pm2.31\times10^{-01}$)	7.17×10^{-01} ($\pm2.02\times10^{-01}$)	1.05 ($\pm2.72\times10^{-01}$)	6.28×10^{-01} ($\pm1.60\times10^{-01}$)	8.86×10^{-01} ($\pm2.26\times10^{-01}$)	7.97×10^{-01} ($\pm2.04\times10^{-01}$)	7.78×10^{-01} ($\pm1.96\times10^{-01}$)	9.73×10^{-01} ($\pm2.45\times10^{-01}$)	5.38×10^{-03} ($\pm1.41\times10^{-03}$)
P2-E2	10.0	2.64×10^{-01} ($\pm7.38\times10^{-02}$)	3.86×10^{-01} ($\pm1.08\times10^{-01}$)	5.08×10^{-01} ($\pm1.31\times10^{-01}$)	3.54×10^{-01} ($\pm9.04\times10^{-02}$)	5.05×10^{-01} ($\pm1.29\times10^{-01}$)	4.48×10^{-01} ($\pm1.15\times10^{-01}$)	4.06×10^{-01} ($\pm1.03\times10^{-01}$)	3.70×10^{-01} ($\pm9.33\times10^{-02}$)	9.15×10^{-04} ($\pm2.57\times10^{-04}$)
P3-E2	10.0	8.16×10^{-01} ($\pm2.18\times10^{-01}$)	7.06×10^{-01} ($\pm1.96\times10^{-01}$)	1.00 ($\pm2.58\times10^{-01}$)	6.38×10^{-01} ($\pm1.63\times10^{-01}$)	8.99×10^{-01} ($\pm2.30\times10^{-01}$)	7.37×10^{-01} ($\pm1.88\times10^{-01}$)	7.35×10^{-01} ($\pm1.85\times10^{-01}$)	8.54×10^{-01} ($\pm2.15\times10^{-01}$)	1.75×10^{-03} ($\pm4.89\times10^{-04}$)
P1-E3	11.0	3.18 ($\pm8.12\times10^{-01}$)	3.01 ($\pm7.93\times10^{-01}$)	3.32 ($\pm8.58\times10^{-01}$)	2.97 ($\pm7.68\times10^{-01}$)	1.19 ($\pm3.03\times10^{-01}$)	1.12 (±3.39)	3.21 ($\pm8.18\times10^{-01}$)	7.84×10^{-01} ($\pm1.98\times10^{-01}$)	2.87×10^{-03} ($\pm8.10\times10^{-04}$)
P2-E3	11.0	2.47 ($\pm6.33\times10^{-01}$)	2.27 ($\pm6.04\times10^{-01}$)	2.41 ($\pm6.26\times10^{-01}$)	2.19 ($\pm5.64\times10^{-01}$)	1.11 ($\pm2.82\times10^{-01}$)	1.06 ($\pm3.29\times10^{-01}$)	2.20 ($\pm5.62\times10^{-01}$)	6.71×10^{-01} ($\pm1.69\times10^{-01}$)	5.63×10^{-03} ($\pm1.54\times10^{-03}$)
P3-E3	11.0	2.52 ($\pm6.43\times10^{-01}$)	2.20 ($\pm5.77\times10^{-01}$)	2.58 ($\pm6.66\times10^{-01}$)	2.25 ($\pm5.81\times10^{-01}$)	1.02 ($\pm2.60\times10^{-01}$)	9.37×10^{-01} ($\pm2.74\times10^{-01}$)	2.48 ($\pm6.30\times10^{-01}$)	5.72×10^{-01} ($\pm1.44\times10^{-01}$)	$<3.41\times10^{-04}$ ($\pm8.61\times10^{-05}$)[a]
P1-E4	12.0	8.98 (±2.27)	9.26 (±2.36)	8.98 (±2.34)	8.17 (±2.27)	7.12×10^{-01} ($\pm1.81\times10^{-01}$)	7.13×10^{-01} ($\pm1.99\times10^{-01}$)	8.21 (±2.07)	5.86 (±1.48)	9.23×10^{-04} ($\pm2.33\times10^{-04}$)
P2-E4	12.0	6.52 (±1.65)	9.86 (±2.51)	4.80 (±1.30)	4.77 (±1.26)	7.78×10^{-01} ($\pm1.98\times10^{-01}$)	8.38×10^{-01} ($\pm2.33\times10^{-01}$)	5.00 (±1.26)	3.88 ($\pm9.80\times10^{-01}$)	2.48×10^{-03} ($\pm6.25\times10^{-04}$)
P3-E4	12.0	1.40×10^{01} (±3.55)	1.26×10^{01} (±3.19)	1.15×10^{01} (±2.98)	1.05×10^{01} (±2.97)	6.62×10^{01} ($\pm1.68\times10^{-01}$)	6.83×10^{-01} ($\pm1.95\times10^{-01}$)	1.01×10^{01} (±2.54)	7.17 (±1.81)	$<4.08\times10^{-04}$ ($\pm1.03\times10^{-04}$)[a]

[a] Maximum rate of dissolution determined from analyte detection threshold value.

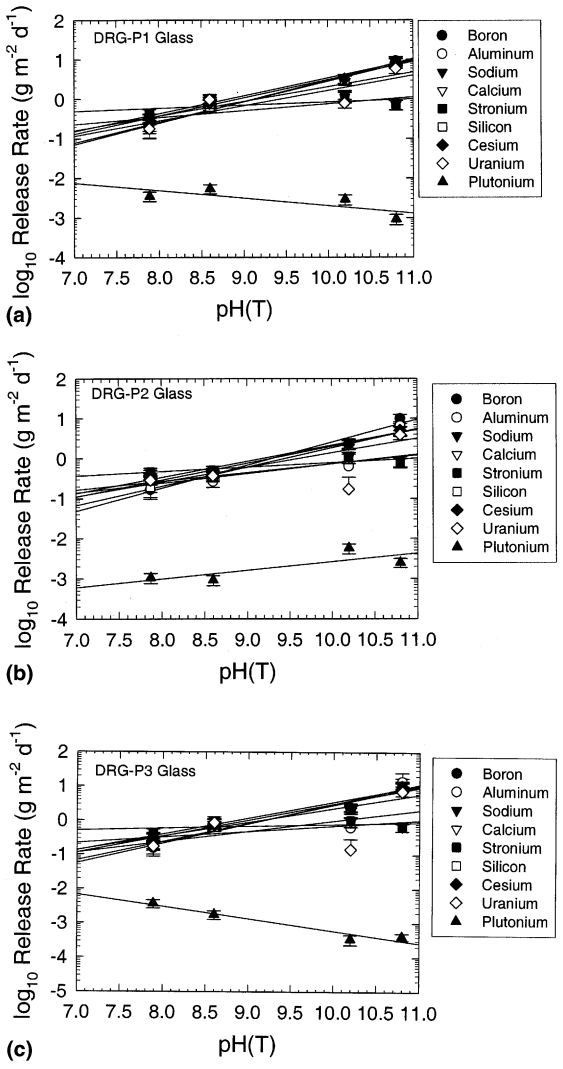

Fig. 4. Plot of $\log_{10}$ dissolution rate indexed by release of Al, B, Ca, Cs, Na, Pu, Si and U for: (a) DRG-P1 (1.0 wt% ^{239}Pu) glass; (b) DRG-P2 (0.9 wt% ^{239}Pu, 0.1 wt% ^{238}Pu) glass, and (c) DRG-P3 (1.0 wt% ^{238}Pu) glass.

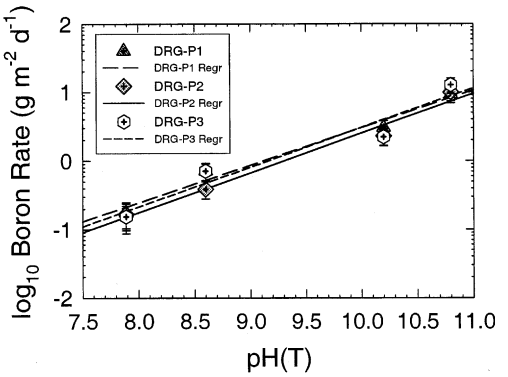

Fig. 5. Dissolution rate ($\log_{10}$) based on boron versus temperature-corrected pH for DRG-P1, -P2 and -P3 glasses. The release rate of boron is the same within experimental uncertainty irrespective of glass composition. The average slope of the lines regressed through the data points yields the dimensionless pH power law coefficient (0.57 ± 0.05).

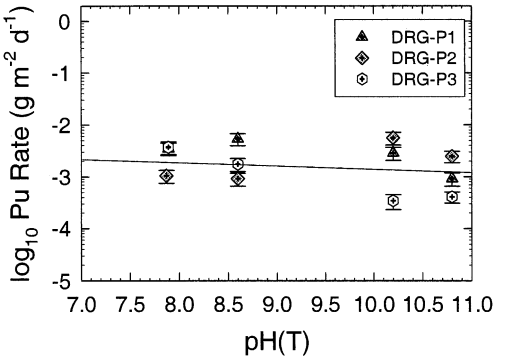

Fig. 6. Log_{10} plutonium dissolution rate versus temperature corrected pH for DRG-P1, -P2 and -P3 glasses.

increasing pH. Importantly, release of Pu to solution is identical within experimental uncertainty for all glass compositions at each pH (Fig. 6). These data are interpreted as evidence for a similar mechanism controlling Pu release from all three glasses, irrespective of radiation damage. In summary, the constant concentrations of Ca, Pu and Sr over the pH range are consistent with solubility control.

5.2. SEM-EDS observations

An analysis of an un-reacted ^{238}Pu-bearing glass coupon (Fig. 7(a)) by SEM methods revealed uncharacterized non-homogeneities that might be attributable to phase separation, but no Pu-bearing crystals were observed. In contrast, the SEM-EDS analyses of reacted coupons record the presence of Pu-rich material on the reacted glass surfaces (Fig. 7(b)–(c)). Other secondary phases include Fe- and Mn-oxyhydroxides. The intense radiation field produced by plutonium coupled with the small size of the Pu-rich objects rendered it impossible to completely characterize all of the surface precipitates. However, partial EDS analyses indicate that there is no discernible Pu associated with iron-rich precipitates (Fig. 8(a)). Rather, the areas of concentrated plutonium are associated with Mn-rich areas located within surface etch pits and micro-cracks (Fig. 8(b)). It is, therefore, likely that the specks of plutonium-rich material formed during the reaction process.

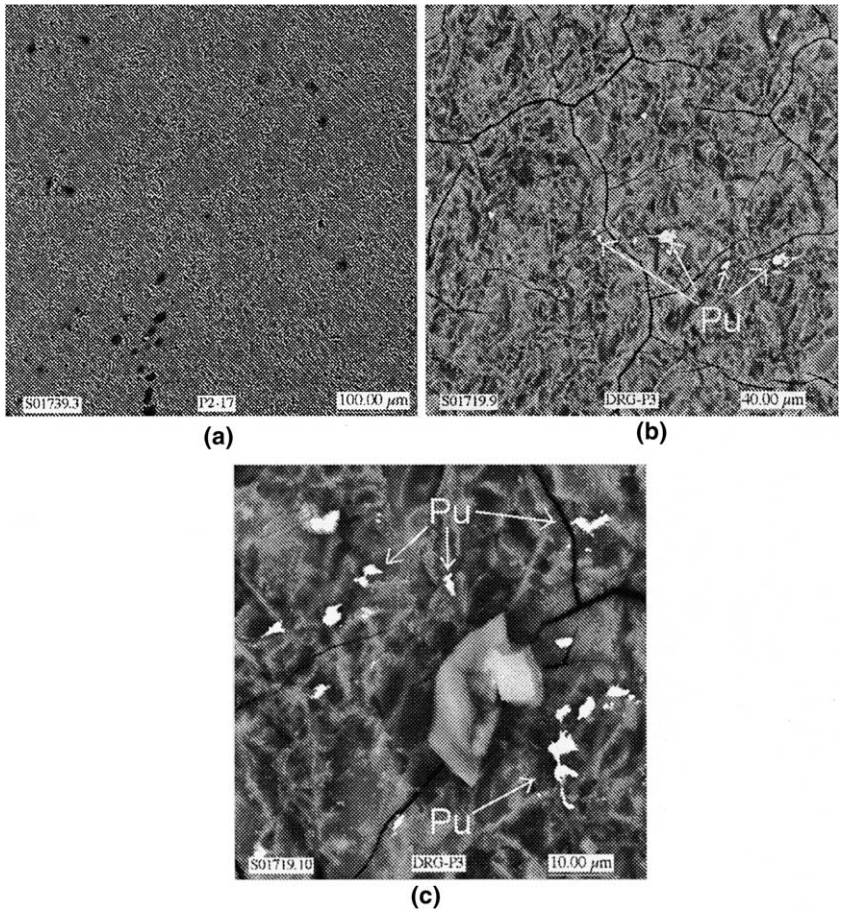

Fig. 7. (a) SEM photomicrograph of non-reacted DRG-P2 glass coupon. The image displays uncharacterized inhomogenities, but no surface Pu-crystals. (b) SEM image of reacted DRG-P3 glass coupon illustrating micro-cracking of the glass surface and concentrated areas of Pu-bearing precipitate, (c) Enhanced SEM image of reacted DRG-P3 glass coupon displaying formation of concentrated Pu-bearing regions and Pu-absent secondary precipitates (EDS shown in Fig. 7(b)). Note 7(c) is *not* an enlarged or magnified view of any area shown in 7(b).

6. Discussion

6.1. Mobility of Cs, Sr and U from boro silicate glass

Subsurface transport of Cs, Sr and U are key risk drivers for assessing the suitability of a geologic burial facility for long-term waste disposal. The data reported herein indicate that in dilute solutions release of Cs will occur at the same rate as glass matrix components, such as Al, B and Si. Because most of the elements from the glass are released at the same rate, it is likely that the glass is dissolving near the forward rate of reaction. Although it is implausible that the dissolution of waste glass in a geologic repository will occur under dilute solution conditions, the rate of Cs release represents the maximum release at the conditions of the experiments.

Compared to Cs release, U rates are identical, except at pH(23 °C) = 11, as pointed out above. Thus, release of U in these experiments is also likely at the forward rate and apparently is influenced by the strong interaction of U with aqueous anionic species. Dissolved uranium, which is present under oxidizing conditions as the uranyl cation (UO_2^{2+}), is complexed by hydroxide and carbonate anions to yield a number of anionic uranyl-hydroxide and -carbonate species. The anionic nature of aqueous uranium species under alkaline conditions hinders sorption to any silica-rich material that may be present as a result of glass dissolution or spallation [26]. However, geochemical modeling (MINTEQA2) [27] indicates that the concentration of calcium and strontium reached solubility limits for $CaUO_4$ and $SrUO_4$ across the entire pH range investigated. Solubility limits with respect to uranium hydroxide and carbon-

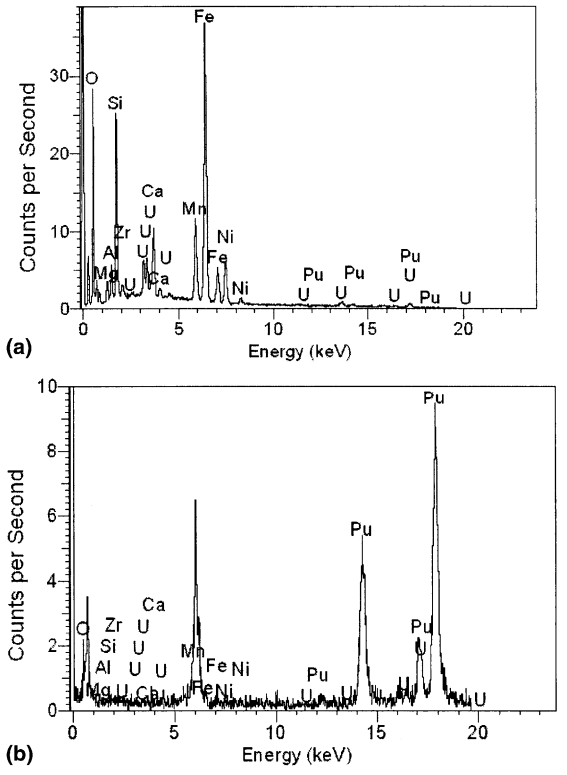

Fig. 8. (a) Partial EDS analysis of secondary Fe-rich precipitate shown in Fig. 7(c) and (b) partial EDS analysis of concentrated Pu-bearing material on reacted glass surface shown in Fig. 7(c).

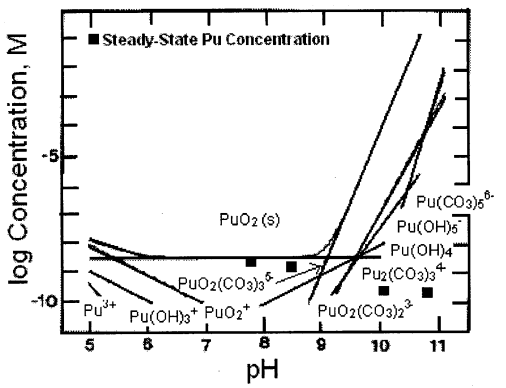

Fig. 9. Plutonium solubility in equilibrium with atmospheric carbon dioxide, $pCO_2 = 10^{-3.5}$ atm (adapted from [32]). Experimental concentrations (depicted as filled squares) are within saturation range with respect to plutonium-hydroxide and -carbonate species under all pH conditions investigated.

ate are also met. Yet, with the exception of the relatively slow rates at pH(23 °C) = 11, there is no evidence that U rates are slower than those for Al, B, Cs, Na, or Si. Because the U rate is systematically low at this pH for all three glass compositions, it is likely due to an experimental artifact.

6.2. Mobility of Pu released from borosilicate glass

Waste glass dissolution generally results in actinide colloid formation from spallation of the waste glass surface layer [8]. In addition, alkaline pH conditions are conducive to the formation of actinide colloids [28], generally ascribed to the 1 nm to 1 μm size-fraction. Polyvalent cations such as plutonium have been shown to readily form colloids composed of hydroxyo complexes [28,29] and Pu-oxides [30]. If the colloids were immobilized by gravitational settling, by electrostatic attraction to the glass surface or reactor walls, or by trapping in surface pits, cracks, or narrow interstices between grains, apparent concentrations of Pu would be diminished. On the other hand, the very limited solubility of Pu could result in formation of secondary plutonium minerals. Therefore, the very low concentrations of Pu (<1 μg/L) in effluent solutions reflect either formation of non-mobile colloids or precipitation of solubility controlling solids.

The possibility of colloid formation was tested by filtering the effluent samples through a 0.45 μm Nalgene® filter. There was no observable difference, within analytical uncertainty, in effluent concentrations between the filtered and unfiltered samples. These results argue against Pu colloids of typical size. However, previous studies of Pu-bearing colloids in the environment and within laboratory experiments have shown that colloids can be smaller than the 0.45 μm size fraction filters used in this study [31]. Thus, Pu-bearing colloids can be separated from solution only through ultra-filtration (<0.4 μm to >500 MW pore size membranes) [26,31]. No attempt to subject solutions to ultra-filtration was made during the course of this investigation. Thus, the presence of nano-colloidal particles (<0.45 μm) cannot be completely excluded.

Comparison of experimental steady-state concentrations to plutonium solubility diagrams at the experimental conditions indicate the system was saturated with respect to aqueous Pu- hydroxide and carbonate species at all experimental pH values (Fig. 9) [32]. In addition, the EDS spectra indicate an association between Pu and Mn. Because of the high residual charge associated with potential plutonium species, electrostatic repulsion may prove a hindrance to colloidal aggregation, thus producing local solubility exceeding that of the solubility product [32]. However, Mn-oxyhydroxides are known to be favorable substrates for sorption of Pu [32,33]. The apparent association between Pu and Mn, as revealed by SEM-EDS characterization, accords with previous observations of an affinity between the two elements. Therefore, the presence of small (<5 μm) discreet Pu-bearing phases that are associated with manganese

oxides likely controls the very low concentrations of Pu in solution.

6.3. The link between internal radiation damage and dissolution rates

Previous investigations have implied that radiation-damaged glass may dissolve faster than unmodified glass, as discussed in the Introduction. Although past dissolution experiments yield conflicting results, other investigations on actinide-bearing glass yield observations that give reason to suspect that rate acceleration is possible. First, spectroscopic data indicate that the local environments around actinide elements change as a result of self-radiation damage. X-ray absorption fine structure (XAFS) spectroscopy studies of the radioactively aged, Pu-bearing glasses tested in this investigation reveal an increase in disorder and bond lengths of oxide polyhedra [34,35] with increasing dose. Weber et al. [36] and references therein show the stored energy of glass increases with increasing cumulative alpha decay dose. Although the change in stored energy becomes constant at higher cumulative doses, the amount of stored energy can be significant (>100 J/g), which may result in the glass becoming more soluble and, therefore, less durable to aqueous attack. Second, glasses containing alpha-emitting radionuclides undergo a small, but measurable, density change over time. The stress induced by density changes, unless annealed at high temperatures, could cause an increase in reactive surface area due to cracking and fracturing of the glass. Third, radiation may induce phase separation, in which two or more distinct glass composition domains form from a homogeneous glass. Typically, the two glass compositions that form from homogeneous silicate glass include a low-, relatively non-durable and a high-silicon, relatively durable, phase. Depending on relative volumes and the connectivity of the low durability glass, the dissolution kinetics will be governed by the least corrosion resistant phase, as demonstrated by McGrail et al. [37]. Of particular concern is the possibility that actinide elements may preferentially partition into the non-durable low silicon phase, which would result in fast release (although actinide solubility limitations would still be enforced). Fourth, radiolysis of water will yield reactive molecules, such as peroxide (H_2O_2), which could enhance release rates. Formation of hydrogen gas (H_2) by radiolysis of water may also result in accelerated release rates if H_2 escapes and leads to high Eh conditions.

If radiation damage affects dissolution rates, boron release data compared between the three glasses should show a progressive increase in rate with greater accumulated dose; i.e., an increase from DRG-P1 to DRG-P3. Because boron is integral to the polymerized silicate glass network and because it is not sequestered by secondary phases after release, rates based on the release of boron best represent the glass dissolution rate. Fig. 5 illustrates the dependence of the dissolution rate (in $\log_{10}$ values) on solution pH(T) based solely on B release. Fig. 5 clearly demonstrates that at each pH value the glass dissolution rates of all three compositions are identical within experimental uncertainty. Therefore, the glass dissolution rates are the same, irrespective of accumulated radiation damage.

Subjecting an amorphous solid such as glass, which consists of various bond lengths, to radiation may result in further changes to bond character. However, given the varying number of bond lengths and angles already present it is not expected that there would be any significant contribution to the overall free energy of formation. Therefore, there would be no measurable effect of radiation damage on the dissolution rate of glasses. Likewise, the increase in volume that is observed in the DRG-P3 glass [38] can result in some increased ion mobility and release, but under the present experimental conditions where the glass is dissolving at the forward reaction rate, any increased ion mobility has a negligible affect on the dissolution rate.

Despite the lack of evidence for a difference in dissolution rate between the glasses at their present level of radiation damage, there is a possibility that changes in aqueous durability occurred at lower degrees of self-radiation damage. In other words, the sensitivity of glass to radiation damage may have been manifested early in its damage history and would have been noticeable if dissolution tests had been run earlier. This possibility follows from analogy to changes in stored energy with accumulated dose. It has been documented that stored energy increases at relatively low accumulated doses, but then becomes constant at higher doses (c.f. Figs. 9 and 10 in [36]). Because the time in which such sensitivity has lapsed, it would not be possible to detect differences in rate between more aged radiation-damaged specimens.

In order to evaluate this possibility, the $\log_{10}$ dissolution rate of a large set of non-radioactive borosilicate glasses was plotted versus the calculated ΔG_{hyd} of glass, as described by Jantzen [39] (Fig. 10; data from [24]). In this algorithm, the contribution of free energy of hydration is summed as a linear combination proportional to the mole fraction of the oxides in the glass. Jantzen [39] proposes that ΔG_{hyd} is a measure of the aqueous durability of the glass; the more positive the value, the greater the corrosion resistance. The average dissolution rate of the DRG-P glasses were normalized to pH 9 and 40 °C, as described by Icenhower et al. [24]. Additionally, the initial dissolution rate measured by Weber et al. [12] was corrected for pH and included in the graph. If radiation effects caused damage that could increase the dissolution rate early in its history, the DRG-P glasses should plot at faster rates compared to non-radioactive borosilicate glass. Note, however, the average rate of

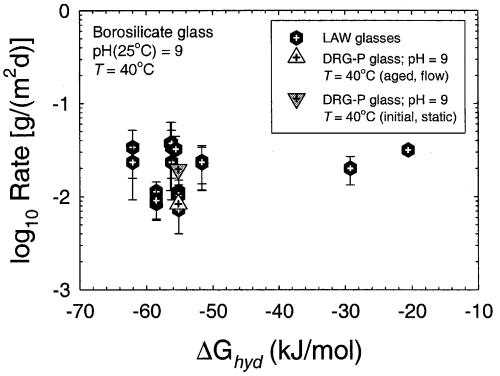

Fig. 10. Plot of the $\log_{10}$ rate (g/(m^2 d)) of non-radioactive 'low activity waste' (LAW) analog glass specimens versus the ΔG_{hyd} of the glass ([39]data from Icenhower et al. [24]). Initial dissolution rate for DRG-P glass specimens were corrected for pH from the original experiment [12]. Rate data for LAW glass were obtained by SPFT methods in chemically dilute solutions in which the forward rate of dissolution was achieved. The data provide strong evidence that release rates exhibit negligible change, irrespective of self-induced radiation damage.

DRG-P glasses plot among data points representing the dissolution rate of non-radioactive borosilicate compositions. Moreover, the pH-corrected initial rate is very close to the dissolution rate values from the radio logically aged specimens. Therefore, the data provide strong evidence that release rates exhibit negligible change over the last ~20 years, irrespective of self-induced radiation damage and the dissolution rates of the Pu-bearing glasses reported in this study are typical for all three glasses throughout its approximate two-decade history.

7. Conclusions

Single-pass flow-through (SPFT) experiments within the pH(23 °C) range of 9–12 and $T = 80$–88 °C on ^{238}Pu and ^{239}Pu-bearing borosilicate glasses indicate that self-radiation damage from alpha decay to the glass network does not affect the dissolution rate. Release rates of elements in this study are subject to solution pH and element solubility. The pH dependence and calculated power law coefficient (0.57 ± 0.04) for each of the glass compositions is consistent with results on other silicate glasses and minerals.

Release of plutonium was invariant with respect to solution pH. SEM analyses revealed concentrated regions of plutonium present within etch pits and microcracks of the reacted glass surface. In addition, geochemical modeling indicates that bulk solutions are saturated with respect to plutonium oxides and hydroxides. Accordingly, we interpret the low mobility of Pu to result from local saturation in Pu-bearing solids immediately after release from glass. However, the crystallinity of Pu-rich areas concentrated in surface features could not be demonstrated and the adsorption and agglomeration of Pu-bearing colloids to the glass surface is a reasonable alternate interpretation.

There are a number of implications from the results of this study. First, self-radiation damage accumulated by a radiologically aged Pu-bearing borosilicate glass does not degrade the corrosion resistance of the material, at least over the accumulated dose range investigated. Second, an increase in borosilicate glass dissolution in an unsaturated repository could result if radiolysis of water and moist air occurs. However, these effects obviously cannot come into play until the metal canister housing the Pu-bearing glass is penetrated by water and air. Third, within a glass-dominated burial facility, where alkaline conditions prevail and ionic strengths are likely to increase as glass dissolution occurs, the concentration of plutonium released from the glass matrix will be minimal due to mineral saturation or agglomeration of colloids. In either case, the mobility of Pu will be strongly curtailed.

Acknowledgments

This work was supported by the Environmental Management Sciences Program, Office of Biological and Environmental Research, US Department of Energy under Contract DE- AC06-76RL01830. We gratefully acknowledge the efforts of K.M Geiszler and S.R. Baum in analyzing effluent samples and thank E.A. Rodriguez, L.A. Snow, R.L. Sell, R.D. Scheele and B.W. Arey for assistance with various aspects of this work.

References

[1] C. Jégou, S. Gin, F. Larche, J. Nucl. Mater. 280 (2000) 216.
[2] T. Advocat, J.L. Chouchan, J.L. Crovisier, C. Guy, V. Daux, C. Jégou, S. Gin, E. Vernaz, Mat. Res. Soc. Symp. Proc. 506 (1998) 63.
[3] A. Barkatt, B.C. Gibson, P.B. Macedo, C.J. Montrose, W. Sousanpour, A. Barkatt, M.-A. Boroomand, V. Rogers, M. Penafiel, Nucl. Technol. 73 (1986) 140.
[4] D.E. Clark, R.L. Schulz, G.G. Wicks, A.R. Lodding, Mat. Res. Soc. Symp. Proc. 333 (1994) 107.
[5] S. Gin, Mat. Res. Soc. Symp. Proc. 412 (1996) 189.
[6] B. Grambow, Mat. Res. Soc. Symp. Proc. 44 (1985) 15.
[7] B.P. McGrail, W.L. Ebert, A.J. Bakel, D.K. Peeler, J. Nucl. Mater. 249 (1997) 175.
[8] V. Pirlet, J. Nucl. Mater. 298 (2001) 47.
[9] E. Vernaz, S. Gin, C. Jégou, I. Ribet, J. Nucl. Mater. 298 (2001) 27.

[10] D.M. Strachan, T.L. Croak, J. Non-Cryst. Solids 272 (2000) 22.
[11] D.J. Wronkiewicz, Mat. Res. Soc. Symp. Proc. 333 (1994) 83.
[12] W.J. Weber, J.W. Wald, H. Matzke, Am. Ceram. Soc. 68 (1985) C253.
[13] L. Werme, I.K. Björner, G. Bart, H.U. Zwicky, B. Grambow, W. Lutze, R.C. Ewing, C. Magrabi, J. Mater. Res. 5 (1990) 1130.
[14] B.P. McGrail, J.P. Icenhower, D.K. Shuh, P. Liu, J.G. Darab, D.R. Baer, S. Thevuthasen, V. Shutthanandan, M.H. Engelhard, C.H. Booth, P. Nachimuthu, J. Non-Cryst. Solids 296 (2001) 10.
[15] T.J. Wolery, EQ3NR, A Computer Program for Geochemical Aqueous Speciation- Solubility Calculations: Theoretical Manual, User's Guide and Related Documentation (version 7.0), UCRL-MA-110662, Lawrence Livermore National Laboratory, Berkley, CA, 1992.
[16] P. Aagaard, H. Helgeson, Am. J. Sci. 282 (1982) 237.
[17] A.C. Lasaga, in: A.F. White, S.L. Brantley (Eds.), Chemical Weathering Rates of Silicate Minerals, Mineralogical Society of America, Washington DC, 1995, p. 23.
[18] P.B. McGrail, P.P. Martin, H.T. Schaef, C.W. Lindenmeier, A.T. Owen, Mat. Res. Soc. Symp. Proc. 608 (2001) 345.
[19] A.B. Kersting, D.W. Efurd, D.L. Finnegan, D.J. Rokop, D.K. Smith, J.L. Thompson, Nature 397 (1999) 56.
[20] W.L. Bourcier, A. Brachmann, LJ. Jardine, C.E. Palmer, V.V. Romanovski, H.F. Shaw, Characterization of Pu Colloidal and Aqueous Species in Yucca Mountain Groundwater Surrogate, UCRL-JC-134460, Lawrence Livermore National Laboratory, Berkley, CA, 1999.
[21] D.M. Strachan, R.D. Scheele, J.P. Icenhower, A.E. Kozelisky, R.L. Sell, V.L. LeGore, H.T. Schaef, M.J. O'Hara, C.F. Brown, W.C. Buchltniller, The status of radiation damage experiments, PNNL-13721, Pacific Northwest National Laboratory, Richland, WA, 2001.
[22] P.B. McGrail, W.L. Ebert, A.J. Bakel, D.K. Peeler, J. Nucl. Mater. 249 (1997) 175.
[23] P.B. McGrail, J.P. Icenhower, P.F. Martin, D.R. Rector, H.T. Schaef, E.A. Rodriguez, J.L. Steele, Low-Activity Waste Glass Studies: FY2000 Summary Report, PNNL-13381, Pacific Northwest National Laboratory, Richland, WA, 2000.
[24] J.P. Icenhower, P.B. McGrail, P. Nachimuthu, D.K. Shuh, E.A. Rodriguez, J.L. Steele, S. Lancaster, L.M. Deskin, Geochim. Cosomochim., submitted for publication.
[25] J.I. Drever, Geochim. Cosomochim. Acta 58 (1994) 2325.
[26] K.H. Lieser, G. Gleitsmann, S. Peschke, T. Steinkopff, Radiochim. Acta 66&67 (1986) 39.
[27] J.D. Allison, D.S. Brown, K.J. Novo-Gradac, MINTEQA2/PRODEFA2, A Geochemical Assessment Model for Environmental Systems: Version 3 User's Manual, EPA/600/3-91/021, Environmental Research Laboratory, Office of Research and Development, US EPA, 1991.
[28] T.C. Maiti, M.R. Smith, J.C. Laul, Nucl. Technol. 84 (1988) 82.
[29] C. Keller, The Chemistry of the Transuranium Elements, Verlag Chemie, Weinheim, 1971.
[30] R.J. Silva, H. Nitsche, Radiochim. Acta 70&71 (1995) 377.
[31] D.L Kaplan, P.M. Bertsch, D.C. Adriano, K.A. Orlandini, Radiochim. Acta 66&67 (1994) 181.
[32] B. Allard, J. Rydberg, Plutonium Chemistry, American Chemical Society, Washington DC, 1983, 275.
[33] W.L. Lindsay, Chemical Equilibria in Soils, John Wiley, Caldwell, New Jersey, 1979, p. 449.
[34] N.J. Hess, W.J. Weber, S.D. Conradson, J. Nucl. Mater. 254 (1998) 175.
[35] N.J. Hess, W.J. Weber, S.D. Conradson, J. Alloys Compd. 271–273 (1998) 240.
[36] W.J. Weber, R.C. Ewing, C.A. Angell, G.W. Arnold, A.N. Cormack, J.M. Delaye, D.L. Griscom, L.W. Hobbs, A. Navrotsky, D.L. Price, A.M. Stoneham, M.C. Weinberg, J. Mater. Res. 12 (1997) 1946.
[37] B.P. McGrail, J.P. Icenhower, E.A. Rodriguez, Mat. Res. Soc. Symp. Proc. 713 (2002) 537.
[38] I. Muller, W.J. Weber, MRS Bulletin 26 (2001) 698.
[39] C.M. Jantzen, Am. Ceram. Soc. 75 (1992) 2433.